

SUPPORTING INFORMATION

Sequential, Low-Temperature Aqueous Synthesis of Ag-In-S/Zn Quantum Dots via Staged Cation Exchange under Biomineralization Conditions

Nur Koncu Ozdemir¹, Joseph P. Cline², John Sakizadeh¹, Shannon M. Collins¹, Angela C. Brown¹, Steven McIntosh¹, Christopher J. Kiely^{1,2}, Mark A. Snyder^{1*}

¹ Dept. of Chemical and Biomolecular Engineering, Lehigh University, Bethlehem, PA 18015,
United States

² Dept. of Materials Science and Engineering, Lehigh University, Bethlehem, PA 18015,
United States

* Corresponding author: snyder@lehigh.edu (M.A. Snyder)

Number of Pages: 9

Number of Figures: 11

Number of Tables: 4

Content

| | |
|--|----|
| A. Supplemental experimental procedures..... | S2 |
| B. AgNO ₃ precursor stability in the aqueous buffered biomineralization system..... | S2 |
| C. Characterization of biomineralized In ₂ S ₃ precursor nanocrystals | S3 |
| D. Characterization of AIS nanocrystals derived from Ag ⁺ exchange in biomineralization media | S4 |
| E. Elucidating photoluminescence decay of AIS and AIS/Zn QD samples..... | S6 |
| F. Characterization of AIS/Zn particles | S7 |
| G. THP-1 macrophages upon incubation with anti-CD11b-conjugated AIS/Zn QDs | S9 |
| H. References..... | S9 |

A. Supplemental experimental procedures

ICP-OES based analysis of Indium(III) concentration in biomineralized In_2S_3 solutions

A diluted biomineralized In_2S_3 solution, cleaned by precipitation-dissolution, was digested in 5% nitric acid (HNO_3 ; Millipore, GR ACS 70%), added gravimetrically. Elemental analysis was carried out on a Spectro Genesis ICP-OES instrument based on In(III), detected at a wavelength of 230.606 nm.

Precipitation-dissolution based cleaning of QDs

QD cleaning was achieved by a precipitation-dissolution based method commonly employed for QD purification.¹ Specifically, QDs were precipitated by the addition of 4 volume equivalents (4V) of 200 proof ethanol to a volume, V, of a synthesis solution containing hydrophilic QDs, followed by i) centrifugation (10,000 rpm, 15 min), ii) supernatant decantation, iii) QD redispersion in 0.1 M Tris buffer (pH 9) by bath sonication (5 min), and iv) filtration (0.45 μm PES syringe filter).

B. AgNO_3 precursor stability in the aqueous buffered biomineralization system

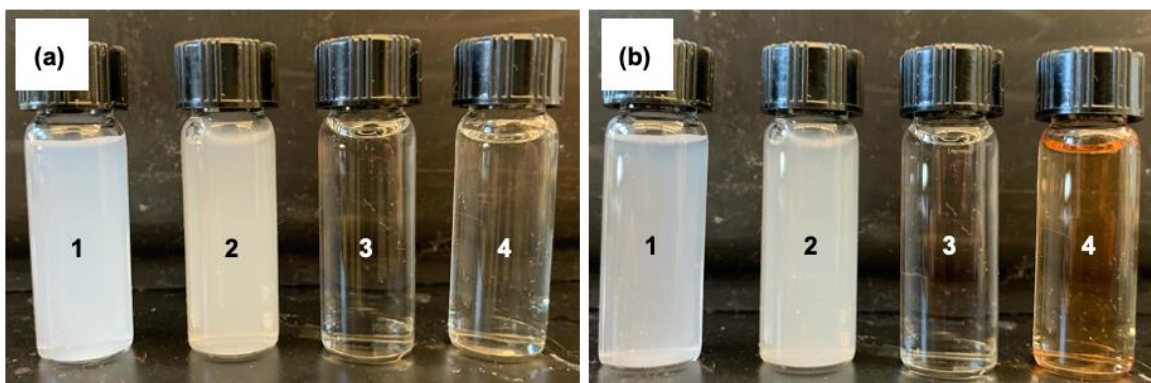


Figure S1. Solutions of 1 mM silver nitrate in 0.1 M Tris-HCl (pH 9.0) buffer for solution compositions containing (1) Ag only, (2) 0.1 mg/ml CSE, (3) 8 mM cysteine, and (4) 8 mM cysteine and 0.1 mg/ml CSE (a) immediately after mixing and (b) after 15 min incubation at room temperature.



Figure S2. Solutions of 1 mM silver nitrate in 0.1 M Tris-HCl (pH 9.0) buffer with Cys/Ag molar ratios of (1) 8, (2) 4, (3) 2, and (4) 1 as a mimic of enzymatic turnover of cysteine.

C. Characterization of biomineralized In_2S_3 precursor nanocrystals

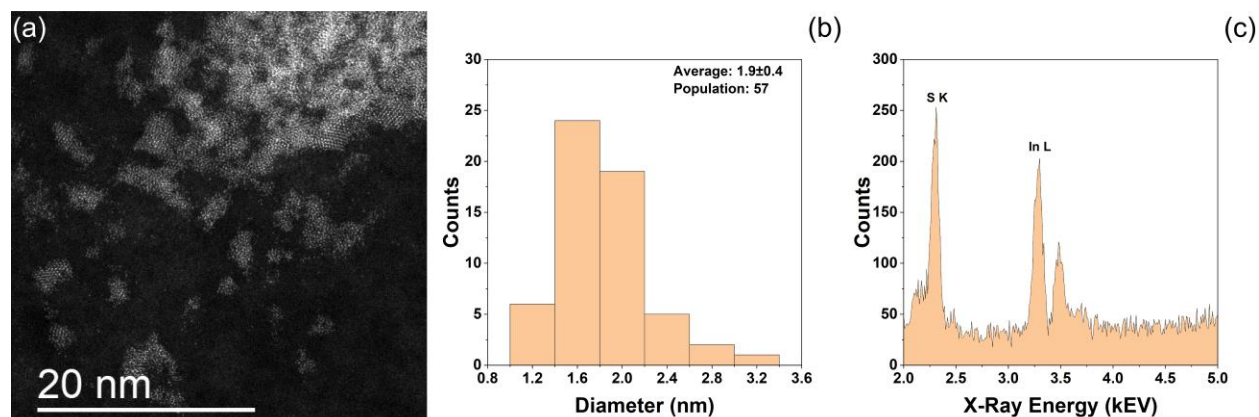


Figure S3. (a) HAADF-STEM image of In_2S_3 particles synthesized by low-temperature biomineralization by the CSE-based turnover of cysteine to HS^- in buffered (pH 9) solutions of indium chloride, along with (b) the measured particle size distribution (PSD), and (c) XEDS data from the region shown in (a) indicating the presence of sulfur and indium.

Table S1. Matching of interplanar spacings and angles for the particle shown in **Figure 1b**, demonstrating the presence of the tetragonal In_2S_3 phase.²

| Plane | Experimental | Theoretical | Error |
|----------|--------------|-------------|--------|
| P1 (215) | 0.294 nm | 0.302 nm | -2.65% |
| P2 (031) | 0.256 nm | 0.253 nm | 1.19% |
| P3 (226) | 0.243 nm | 0.241 nm | 0.83% |
| P1<P2 | 68.7° | 69.0° | -0.43% |
| P1<P3 | 62.0° | 62.7° | -1.12% |

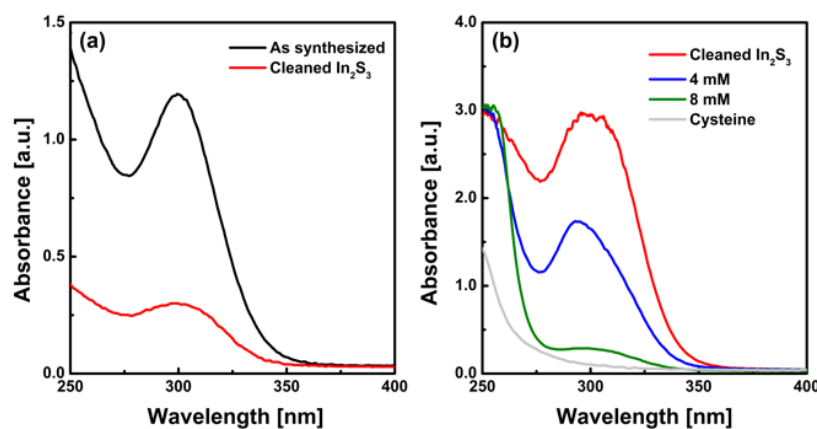


Figure S4. Sensitivity of absorbance measured on In_2S_3 particles (a) before and after precipitation-dissolution cleaning and (b) upon cysteine addition, at concentrations of 4 mM and 8 mM, to initially cleaned In_2S_3 . Background absorbance for cysteine only is shown for reference in (b).

D. Characterization of AIS nanocrystals derived from Ag⁺ exchange in biomineralization media

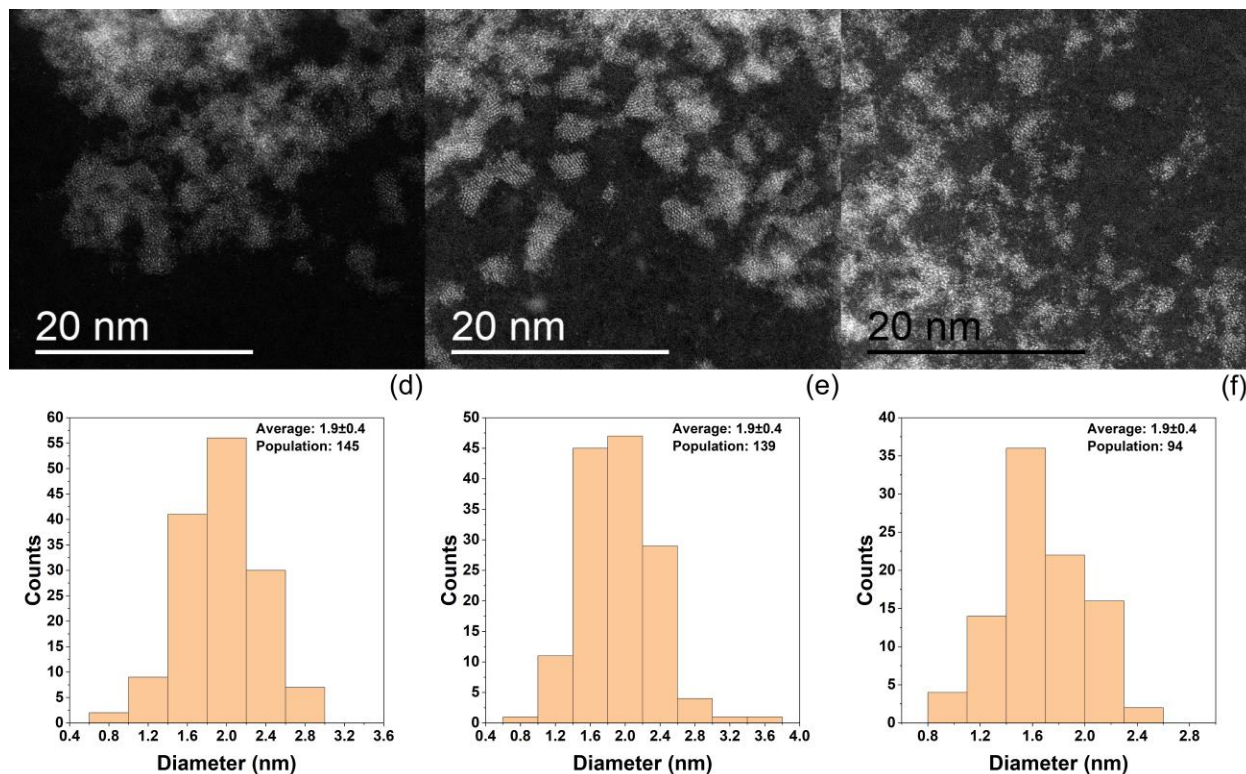


Figure S5. (a-c) Representative HAADF-STEM images and (d-f) measured particle size distributions for AIS particles resulting from 3-day incubation of biomineralized In₂S₃ precursor particles in solutions with In/Ag molar ratios of (a,d) 5, (b,e) 10, and (c,f) 20.

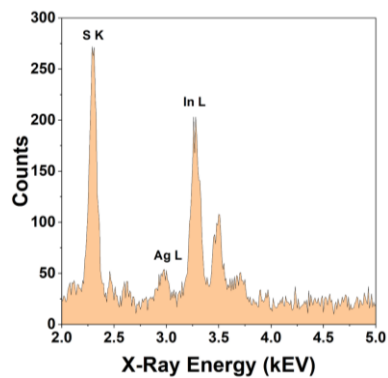


Figure S6. XEDS spectrum for AIS particles resulting from 3-day incubation of biomineralized In₂S₃ precursor particles in solutions with an In/Ag molar ratio of 20.

Table S2. Matching of interplanar spacings and angles for the $[\bar{1}10]$ zone axis shown in **Figure 4(a)** and **(b)**, demonstrating the presence of the cubic AgIn_5S_8 phase for In/Ag~5 and 10 AIS particles, respectively.³

| | Plane | Experimental | Theoretical | Error |
|--------------------|--------------------------|--------------|-------------|--------|
| Figure 4(a) | P1 (222) | 0.312 nm | 0.313 nm | -0.32% |
| | P2 ($2\bar{2}\bar{2}$) | 0.302 nm | 0.313 nm | -3.51% |
| | P3 (004) | 0.282 nm | 0.271 nm | 4.06% |
| | P1<P2 | 65.8° | 70.5° | -6.67% |
| | P1<P3 | 54.5° | 54.7° | -0.37% |
| | P2<P3 | 124.2° | 125.3° | -0.88% |
| Figure 4(b) | P1 (222) | 0.320 nm | 0.313 nm | 2.24% |
| | P2 (004) | 0.266 nm | 0.271 nm | -1.85% |
| | P3 (226) | 0.161 nm | 0.163 nm | -1.23% |
| | P1<P2 | 56.6° | 54.7° | 3.47% |
| | P1<P3 | 30.2° | 29.5° | 2.37% |
| | P2<P3 | 26.4° | 25.2° | 4.76% |

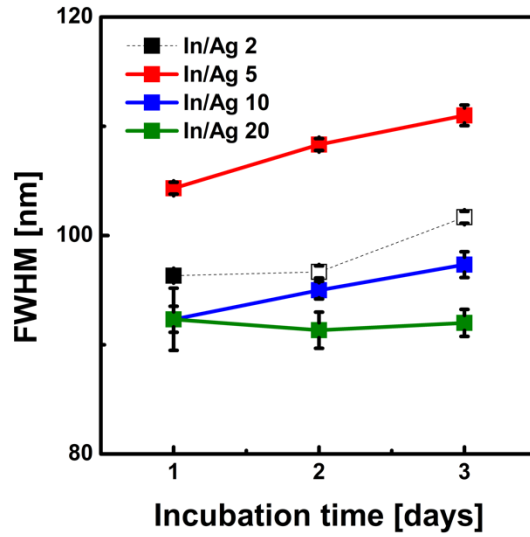


Figure S7. The effect of In/Ag ratio and incubation time on the FWHM of the PL emission spectra. Stable and unstable solutions are differentiated by closed symbols/solid lines and open symbols/dashed lines, respectively.

E. Elucidating photoluminescence decay of AIS and AIS/Zn QD samples

Table S3. Bi-exponential fitting of photoluminescence (PL) decay curves collected for AIS QDs resulting from 1-day (AIS-1d), 2-day (AIS-2d), and 3-day (AIS-3d) incubation of biomineralized In₂S₃ NCs in solutions of In/Ag~5, compared with AIS QDs synthesized by 3-day incubation in solutions with In/Ag~10 (In/Ag 10) and 20 (In/Ag 20) as well as Zn-incorporated AIS QDs (AIS/Zn). Decay curves were fitted according to:

$$I(t) = B_1 \exp(-t/\tau_1) + B_2 \exp(-t/\tau_2),$$

where B_1 and B_2 are respective weights of the fast and slow exponential decay terms, with corresponding characteristic times of τ_1 and τ_2 . All fits have Chi-squared < 1.2. The average PL lifetime is computed as:

$$\tau_{avg} = (B_1 \times \tau_1 + B_2 \times \tau_2)/(B_1 + B_2).$$

| Sample | Incubation time [days] | In/Ag | τ_1 (ns) | τ_2 (ns) | B_1 (%) | B_2 (%) | τ_{avg} (ns) |
|------------------|------------------------|-------|---------------|---------------|------------|------------|-------------------|
| AIS-1d | 1 | 5 | 5.02±0.06 | 39.27±0.57 | 9.23±0.10 | 90.77±0.10 | 36.11±0.50 |
| AIS-2d | 2 | 5 | 5.32±0.10 | 37.42±1.26 | 4.09±0.14 | 95.91±0.14 | 36.10±1.18 |
| AIS-3d (In/Ag 5) | 3 | 5 | 4.29±0.61 | 50.16±1.92 | 2.74±0.17 | 97.26±0.17 | 48.92±1.88 |
| In/Ag 10 | 3 | 10 | 2.62±0.96 | 33.98±5.51 | 6.74±0.32 | 93.26±0.32 | 31.89±5.26 |
| In/Ag 20 | 3 | 20 | 6.53±4.93 | 11.33±4.36 | 45.31±9.06 | 54.69±9.06 | 11.35±1.06 |
| AIS/Zn | 3 | 5 | 2.70±1.10 | 76.48±12.07 | 1.43±0.21 | 98.57±0.21 | 75.49±12.06 |

F. Characterization of AIS/Zn particles

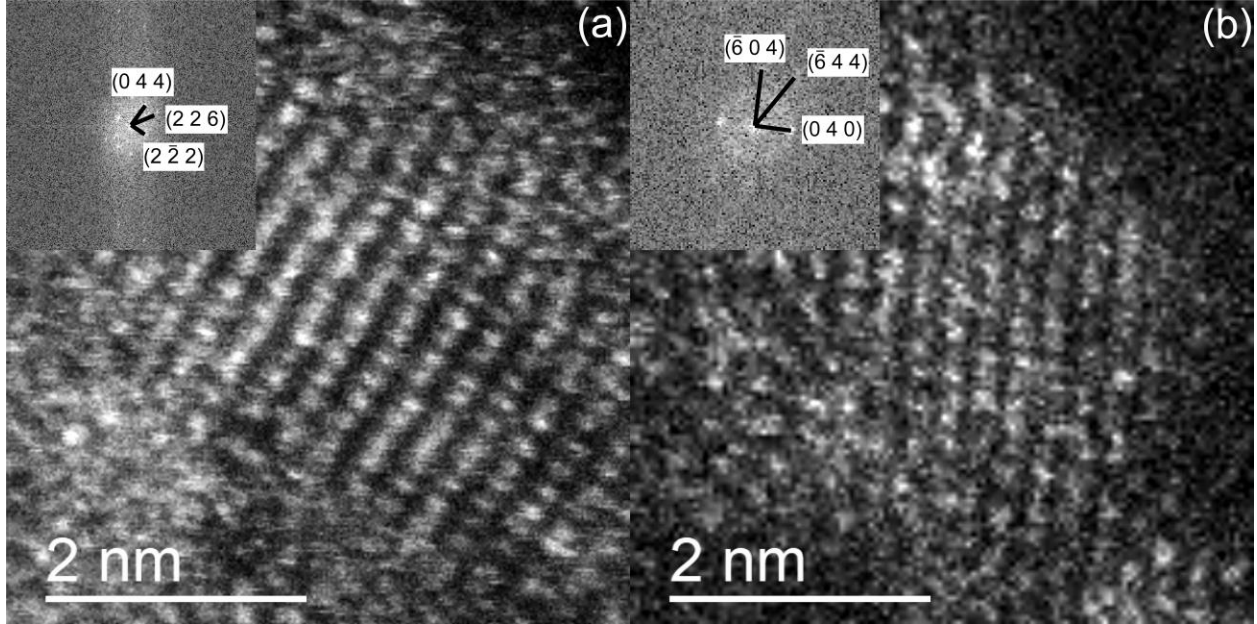


Figure S8. Representative HAADF-STEM images and indexing of Zn-incorporated AIS QDs along the (a) $[\bar{2}\bar{1}1]$ and (b) $[203]$ zone axes for the cubic AgIn_5S_8 structure.

Table S4. Matching of interplanar spacings and angles for the Zn-incorporated AIS/Zn particles shown in **Figure 6d** for the $[\bar{1}10]$ zone axis and **Figure S8** for the $[\bar{2}\bar{1}1]$ and the $[203]$ zone axes of the cubic AgIn_5S_8 structure.

| | Plane | Experimental | Theoretical | Error |
|--------------|--------------------------------|--------------|-------------|--------|
| Figure 6(d) | P1 ($2\bar{2}\bar{2}$) | 0.309 nm | 0.313 nm | -1.28% |
| | P2 (222) | 0.301 nm | 0.313 nm | -3.83% |
| | P3 (004) | 0.262 nm | 0.271 nm | -3.32% |
| | P1<P2 | 70.4° | 70.5° | -0.14% |
| | P1<P3 | 58.1° | 54.7° | 6.22% |
| | P2<P3 | 128.1° | 125.3° | 2.23% |
| Figure S8(a) | P1 ($\bar{2}\bar{2}\bar{2}$) | 0.311 nm | 0.313 nm | -0.64% |
| | P2 (044) | 0.185 nm | 0.191 nm | -3.14% |
| | P3 (226) | 0.161 nm | 0.163 nm | -1.23% |
| | P1<P2 | 90.0° | 90.0° | 0.00% |
| | P1<P3 | 56.0° | 58.5° | -4.27% |
| | P2<P3 | 33.1° | 31.5° | 5.08% |
| Figure S8(b) | P1 (040) | 0.264 nm | 0.271 nm | -2.58% |
| | P2 ($\bar{6}04$) | 0.157 nm | 0.150 nm | 4.67% |
| | P3 ($\bar{6}44$) | 0.132 nm | 0.131 nm | 0.76% |
| | P1<P2 | 88.4° | 90.0° | -1.78% |
| | P1<P3 | 58.2° | 60.9° | -4.43% |
| | P2<P3 | 29.9° | 29.0° | 3.10% |

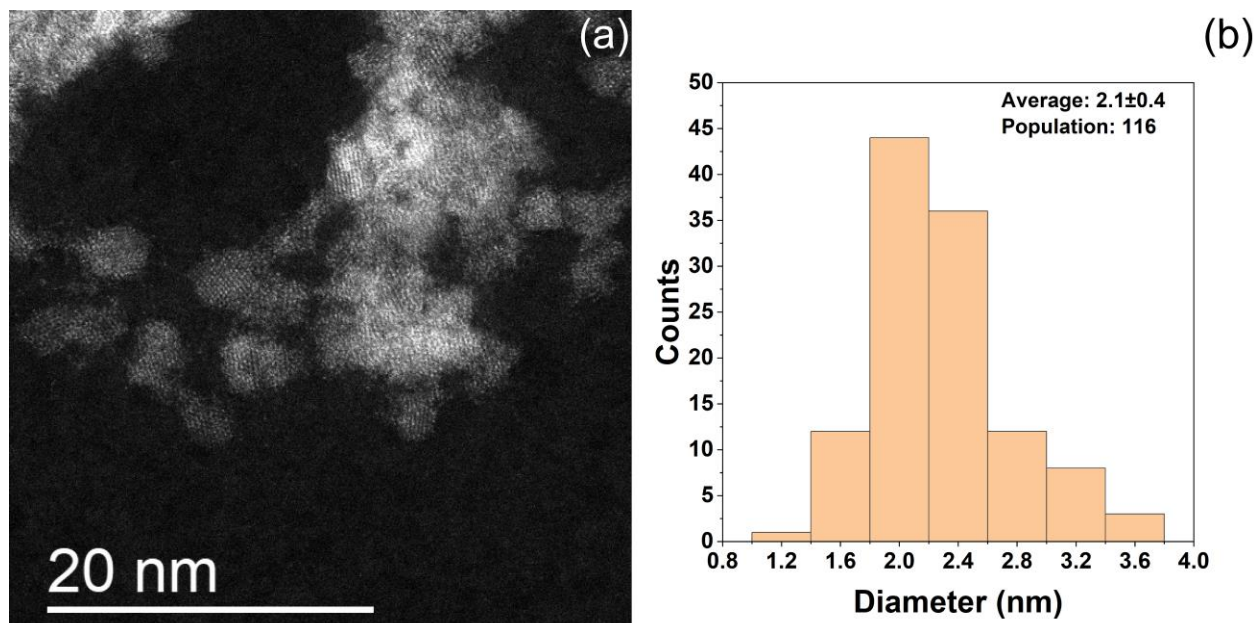


Figure S9. (a) A representative HAADF STEM image of the AIS/Zn QDs. (b) The corresponding particle size distribution derived from this sample.

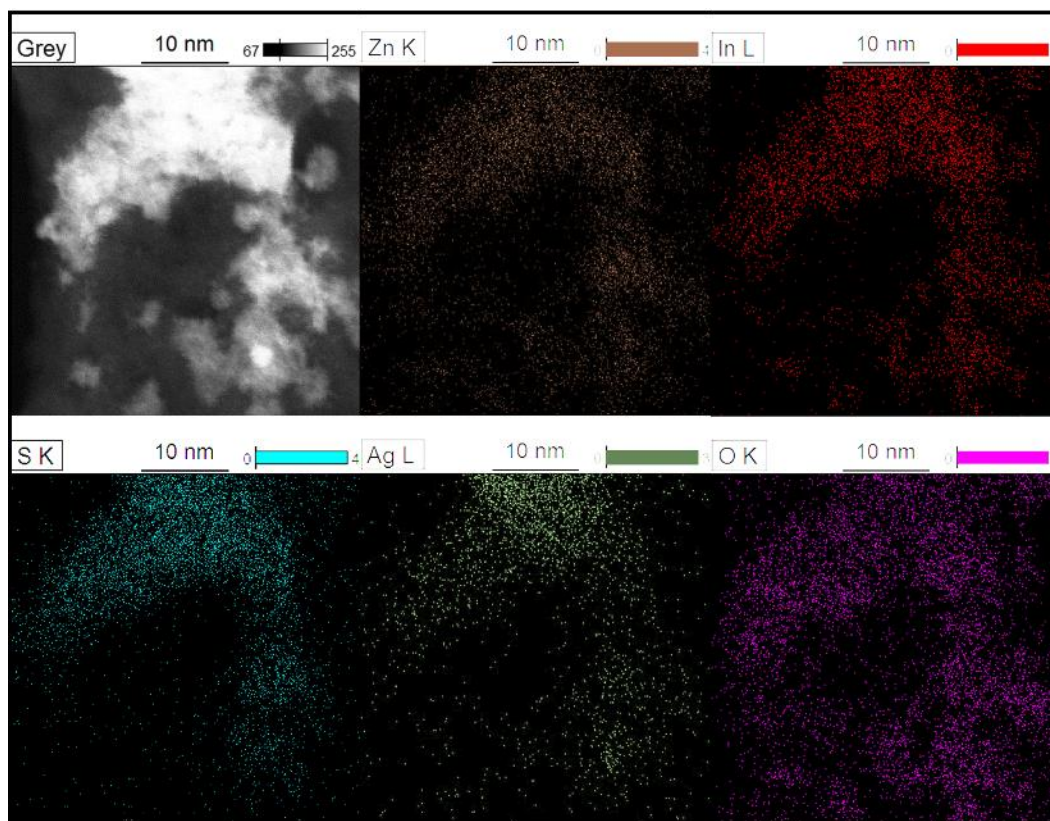


Figure S10. HAADF-STEM image and corresponding Zn, In, S, Ag, and O XEDS elemental maps of the Zn-incorporated AIS QD sample.

G. THP-1 macrophages upon incubation with anti-CD11b-conjugated AIS/Zn QDs

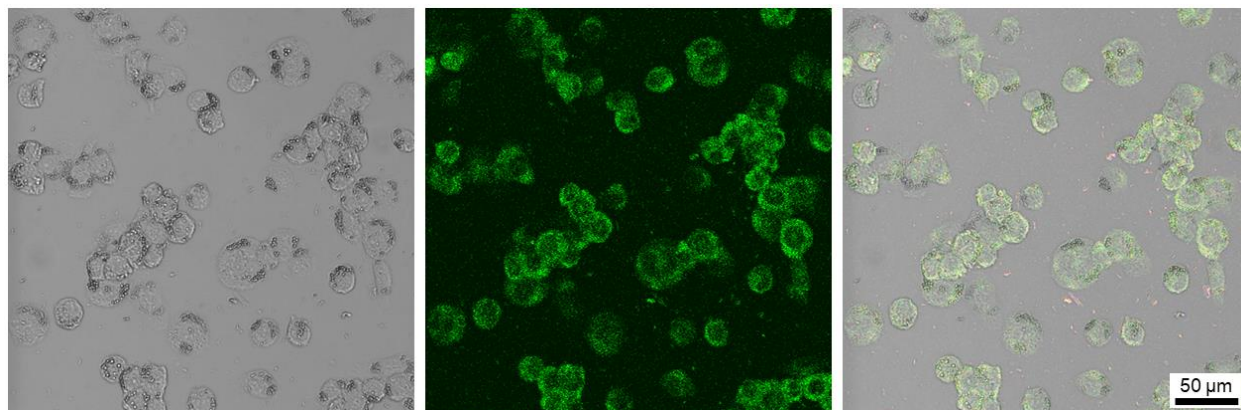


Figure S11. 2D fluorescence confocal optical slice alone and merged with bright-field images of a representative field of THP-1 macrophages following their incubation with anti-Cd11b-conjugated AIS/Zn QDs.

H. References

- (1) Lim, H.; Woo, J. Y.; Lee, D. C.; Lee, J.; Jeong, S.; Kim, D. Continuous Purification of Colloidal Quantum Dots in Large-Scale Using Porous Electrodes in Flow Channel. *Sci. Rep.* **2017**, *7*, 43581. DOI:10.1038/srep43581.
- (2) Pistor, P.; Merino Álvarez, J. M.; León, M.; di Michiel, M.; Schorr, S.; Klenk, R.; Lehmann, S. Structure Reinvestigation of α -, β - and γ -In₂S₃. *Acta Crystallogr. Sect. B* **2016**, *72* (3), 410–415. DOI:10.1107/S2052520616007058.
- (3) Delgado, G.; Mora, A. J.; Pineda, C.; Tinoco, T. Simultaneous Rietveld Refinement of Three Phases in the Ag-In-S Semiconducting System from X-Ray Powder Diffraction. *Mater. Res. Bull.* **2001**, *36* (13), 2507–2517. DOI:10.1016/S0025-5408(01)00741-3.